JOC The Journal of Organic Chemistry

Article

pubs.acs.org/joc

Origin of High Regio-, Diastereo-, and Enantioselectivities in 1,6-Addition of Azlactones to Dienyl *N*-Acylpyrroles: A Computational Study

Masahiro Yamanaka,[*,§] Ken Sakata,[¶] Ken Yoshioka,[†] Daisuke Uraguchi,[†] and Takashi Ooi[†,‡]

[§]Department of Chemistry and Research Center for Smart Molecules, Faculty of Science, Rikkyo University, 3-34-1 Nishi-Ikebukuro, Toshima-ku, Tokyo 171-8501, Japan

[¶]Faculty of Pharmaceutical Sciences, Hoshi University, Ebara, Shinagawa-ku, Tokyo 142-8501, Japan

[†]Institute of Transformative Bio-Molecules (WPI-ITbM) and Department of Applied Chemistry, Graduate School of Engineering, Nagoya University, Nagoya 464-8602, Japan

[‡]CREST, Japan Science and Technology Agency (JST), Nagoya University, Nagoya 464-8602, Japan

Supporting Information

ABSTRACT: Chiral *P*-spiro triaminoiminophosphorane (**1**) was developed to promote the highly regio-, diastereo-, and enantioselective 1,6- and 1,8-additions of azlactones (**2**·H) to dienyl and trienyl *N*-acylpyrroles (**3** and **4**). DFT calculations enabled us to gain deep insight into the whole reaction mechanism as well as the origin of the high regio- and stereoselectivities. The present reaction consists of three steps: (1) formation of the phosphonium-enolate ion-pair complex by deprotonation of **2**·H with **1**, (2) C−C bond formation of **2** with **3** and **4**, and (3) protonation of the resulting enolate anion. The C−C bond formation is irreversible, and the rate- and stereodetermining step. The C^{α}-protonation preferentially proceeds rather than the thermodynamically and kinetically disfavored *O*- and C^{γ}-protonation, respectively. The high regio- and enantioselectivities are mainly attributed to the steric and electronic features of **1**·H and **3**/**4**. The hydrogen bonds (NH−O and CH−O) and the attractive CH−π interaction between **1**·H and **2** and **3** play a key role in achieving high stereocontrol. The high regioselectivity is mainly controlled by the structural distortion of **1**·H and the disruption of the π-conjugated system of **3** (1,4-system) and **4** (1,4- and 1,6-systems).

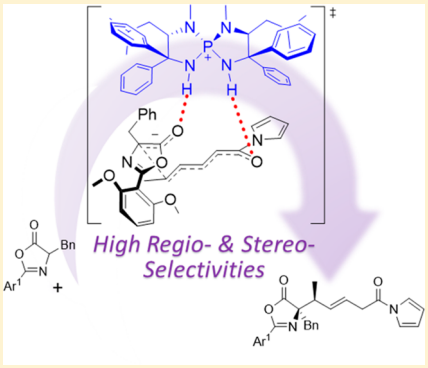

INTRODUCTION

In contrast to the profound understanding of the conjugate addition of carbon nucleophiles such as enolates to α,β-unsaturated carbonyl compounds (Michael reaction),[1] details of a similar conjugate addition to vinylogous acceptors are unclear owing to the lack of studies.[2] This is because the vinylogous electrophiles have two comparably reactive sites at β- and δ-positions to a carbonyl moiety, and their selection in a carbon−carbon bond-forming event is generally difficult.[3] Most of the reported examples use substrates having steric or electronic bias for ensuring regioselectivity, and catalyst-controlled regioselective reactions, particularly the 1,6-addition to $\alpha,\beta,\gamma,\delta$-unsaturated systems, are scarcely reported.[4−8] Some of the present authors have recently reported a highly regio-, diastereo-, and enantioselective 1,6-addition controlled by a catalytic amount of chiral *P*-spiro triaminoiminophosphorane (**1**), in which oxazol-5-(4*H*)-one (**2**·H), i.e., azlactone, and δ-alkyl dienyl *N*-acylpyrroles (**3**) were used as the nucleophile and the electrophile, respectively (Scheme 1).[9] Furthermore, the same catalyst system was found to be highly effective for 1,8-addition of **2**·H to trienyl *N*-acylpyrroles (**4**).[9,10] As the reactive sites of extended Michael acceptors **3** and **4** have similar stereoelectronic properties, the observed complete regioselectivity is facilitated by the core structure and the hydrogen-bonding ability of aminophosphonium cation **1**·H.[11−14] On the other hand, the structures of α-amino acid-derived alkyl substituents (R) on the diazaphosphacycles of **1**·H were found to have a considerable impact on the diastereo- and enantioselectivities in the 1,6-selective reaction, and the isobutyl

Scheme 1. Regio-, Diastereo-, and Enantioselective 1,6- and 1,8-Addition of Azlactones to Dienyl and Trienyl *N*-Acylpyrroles

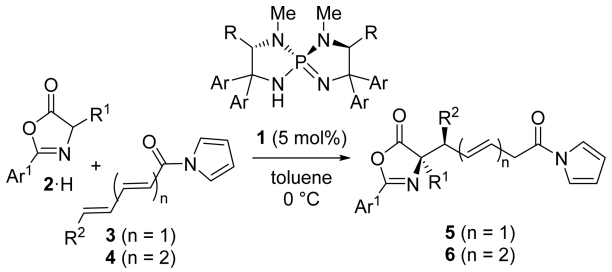

Received: October 25, 2016
Published: December 7, 2016

DOI: 10.1021/acs.joc.6b02572
J. Org. Chem. 2017, 82, 541−548

group was identified to be an optimal substituent.[14] The aromatic substituent (Ar^1) at the 2-position of **2**·H also affects the stereochemical outcome of product **5**. Introduction of the 2,6-dimethoxyphenyl group was finally singled out to afford nearly ideal stereoselectivity.[15] These experimental results have qualitatively indicated the importance of the entire structure of **1**·H. However, quantitative evaluation of the effect of each parameter on the selectivities has not been carried out so far. We describe herein our efforts to gain deep insight into the origin of the high selectivities in the **1**-catalyzed 1,6- and 1,8-additions of **2**·H to **3** and **4** through DFT calculations.

COMPUTATIONAL METHODS

To elucidate the catalytic function of **1**, the reaction mechanism was investigated in detail using a simplified chemical model (Scheme 2a).

Scheme 2. Chemical Models

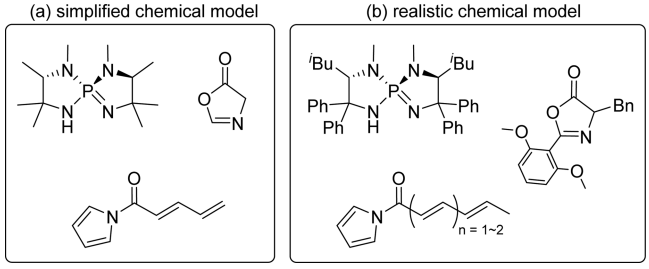

In the simplified chemical model, the R and Ar substituents in **1** were exchanged with Me groups and the R^1 and Ar^1 substituents in **2**·H were removed (by exchanging with H atoms) to reduce computational cost. Focusing on the regio- and stereoselectivity determining C−C bond formation in the 1,6-addition system, diastereomeric transition state (TS) models were compared using a realistic chemical model to clarify the major factor contributing to the asymmetric induction (Scheme 2b). On the basis of the most stable and promising TS structure, the realistic TS models for 1,4-, 1,6-, and 1,8-additions were also addressed to investigate the origin of the high 1,8-selectivity. All calculations were performed with the Gaussian 09 package.[16] Geometries in the simplified chemical model were fully optimized and characterized by frequency calculation at the B3LYP/6-31G* level.[17] Solvation exerts little influence on the energy profile because of the intramolecular chemical transformations (C−C bond formation and protonation) in the unimolecular ion-pair system.[18] For the inclusion of dispersion correction in the realistic chemical model, single-point energy calculations of the optimized structures were conducted at the B3LYP-D3/6-31+G** level.[19] To evaluate more reliable relative Gibbs energies, zero-point energy corrections and thermal and entropic corrections calculated at the B3LYP/6-31G* level were added to the electronic energy calculated at the B3LYP-D3/6-31+G** level. The molecular structures were depicted using the CYLview v1.0.561 *β*.[20]

RESULTS AND DISCUSSION

As a preliminary study, the reaction mechanism in the 1,6-addition system was explored using the simplified chemical model (Figures 1 and 2). The experimentally observed linear relationship between the enantiomeric excess of **1** and that of the 1,6-adduct suggests that **1**·H captures and activates **2** and **3** in a monomeric fashion (Experimental Section; Figure S1 in the Supporting Information). At the first step of the present reaction, phosphonium-enolate ion-pair complexes would be formed in equilibrium. *P*-Spiro iminophosphorane (**Cat**) abstracts the proton at the C^4 position in azlactone (**AZ**·H) to form ion-pair complex **CP1** through two-point hydrogen-bonding interaction between the two NH residues in protonated iminophosphorane **Cat**·H and the oxygen atom in enolate anion **AZ**. The introduction of *N*-acylpyrrole (**AC**) results in loss of the enolate coordination with one of the NH residues in **Cat**·H to further form complex **CP2**. In **CP2**, the phosphonium moiety (e.g., HN-P-NH) enables bridging between **AC** and **AZ**. At the next step, the C−C bond formation proceeds through **TS1**, which is the highest in energy and thus regarded as the rate- and stereodetermining step. Recently, Simón and Paton elucidated a related reaction mechanism for the asymmetric nucleophilic addition of nitroalkanes and phosphites to aldehydes catalyzed by *P*-spiro iminophosphorane **1** in their ONIOM QM/MM study.[21] At the final protonation step, there are three possible pathways, namely, *O*-protonation and *C*-protonation at the C^α and C^γ positions of the resulting enolate anion in **CP3**. The *O*-protonation is kinetically favored because of the lowest **TS2a** but affords the thermodynamically less stable *O*-protonated product (**CP4a**). In contrast, the thermodynamically more stable *C*-protonated products are obtained, albeit with their higher energy barriers. Whereas the C^γ-protonated products (**CP4d** and **CP4e**) are thermodynamically more stable than the C^α-protonated products (**CP4b** and **CP4c**), the C^γ-protonation (**TS2d** and **TS2e**) is energetically less favored than the C^α-protonation (**TS2b** and **TS2c**). Both **TS2d** and **TS2e** are, in particular, located at the higher energy level of **TS1**. Two scenarios (shown in red and blue) are observed in C^α- and C^γ-protonation, depending on which of the two NH residues of the phosphonium moiety protonate the resulting enolate anion. In the most facile C^α-protonation, **TS2b** connects from **CP3′** generated through the rotation of the azlactone fragment of **CP3** (e.g., C^γ−C^δ bond rotation) with a small energy loss (ca. 5 kcal/mol activation barrier, $TS_{3-3'}$).[22] **TS2c** directly connected from **CP3** is less stable than **TS2b** due to loss of the strong hydrogen bond between the positively charged NH residue of **Cat**·H and the negatively charged oxygen atom of the resulting enolate anion. In the energetically unfavorable C^γ-protonation, both **TS2d** and **TS2e** are considerably destabilized by the mismatched position between C^γ and the carbonyl oxygen atoms on the two NH residues of **Cat**·H. These computational results using the simplified model indicate that (1) the C−C bond formation (**TS1**) is irreversible at the rate- and stereodetermining step and (2) C^α-protonation (**TS2b** and **TS2c**) is thermodynamically and kinetically more favorable than *O*-protonation (**TS2a**) and C^γ-protonation (**TS2d** and **TS2e**), respectively.[18] To gain deep insight into the high regio- and stereoselectivities, therefore, the diastereomeric TS structures were investigated using the realistic model based on **TS1**.

To identify the notable features of phosphonium ion **1**·H as the stereocontroller, the electrostatic potentials were computed (Figure 3). Four Ph groups (A and B rings) create a considerably narrow and rigid chiral space (shown by dotted purple circle). The two NH residues are not in plane (H−N−N−H dihedral angle: 103°) and are most positively charged to act as acidic sites. Therefore, **1**·H is predicted to tightly capture both substrates on the NH residues and precisely control the regio- and stereochemical outcome through the steric interaction with four Ph groups.

To identify the major factor contributing to the asymmetric induction in the 1,6-addition of **2**·H to **3** catalyzed by **1**, four diastereomeric TS structures corresponding to the facial selection of **2** and **3** [leading to major and minor enantiomers

DOI: 10.1021/acs.joc.6b02572
J. Org. Chem. 2017, 82, 541−548

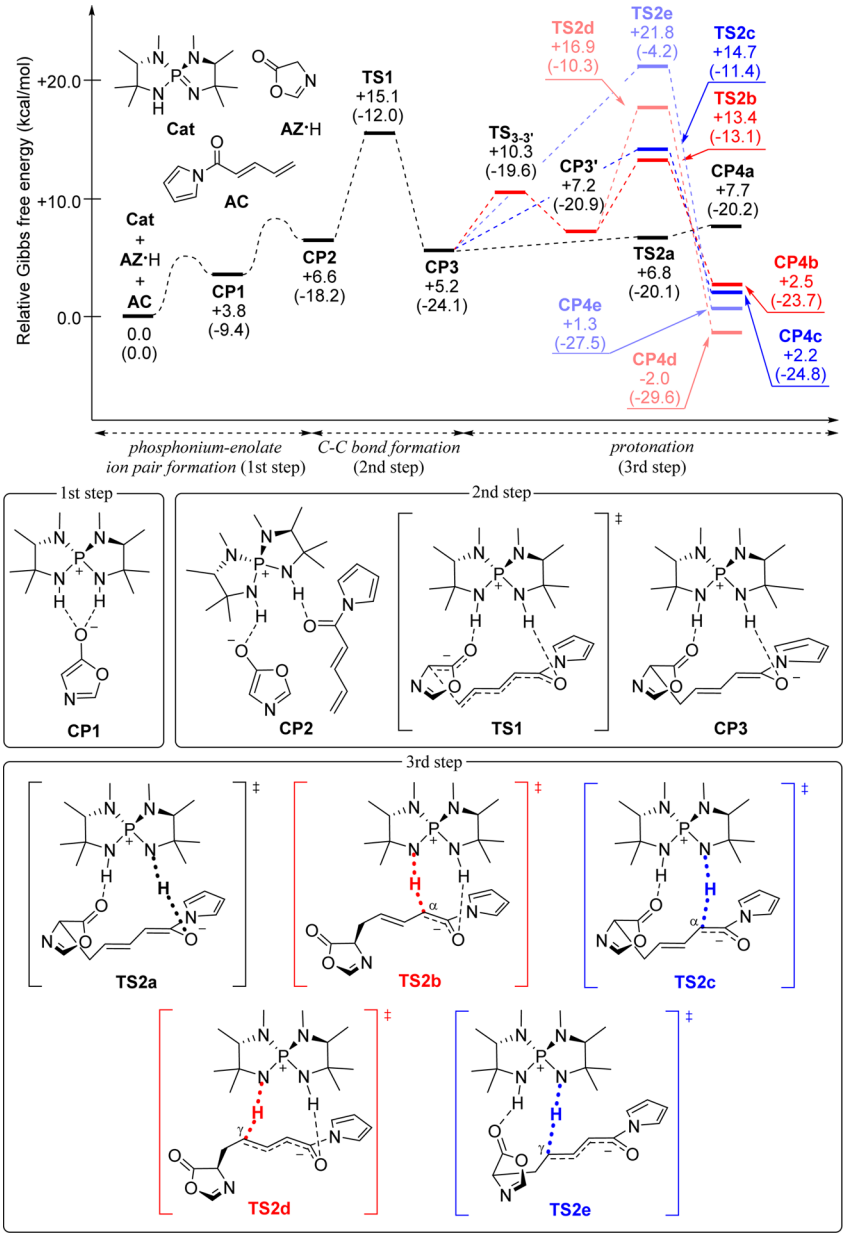

Figure 1. Gibbs energy profile of 1,6-addition of **AZ**·H to **AC** catalyzed by **Cat**. Relative electronic energies are in parentheses (kcal/mol).

(**TS3rs** and **TS3sr**) and minor diastereomers (**TS3ss** and **TS3rr**)] were compared (Figure 4). Whereas **TS3rs** leading to the major enantiomer is the most stable among the four diastereomeric TSs, **TS3sr** leading to the minor enantiomer is 3.9 kcal/mol less stable than **TS3rs**. Diastereomeric **TS3ss** and **TS3rr** are 2.4 and 4.7 kcal/mol less stable than **TS3rs**.[23] These computational results are qualitatively consistent with the experimental results. In all the diastereomeric TSs, both enolate anion **2** and **3** are oriented almost perpendicular to the two Ph groups of **1**·H (A rings in Figure 3) due to the spatial requirement of the narrow space. The dihedral angles of H−N−N−H in the phosphonium center of **1**·H range from 76° to 85° to readily incorporate **2** and **3** in a manner suitable for facilitating 1,6-fashion. Both **2** and **3** fit the chiral space well in the most stable **TS3rs** (Figure 4a).

Therefore, two main NH−O hydrogen bonds are formed between the NH residues of **1**·H and the negatively charged oxygen atoms of **2** and **3** (1.845 and 1.740 Å, respectively) in **TS3rs**. It should be noted that a CH−π interaction (3.033 Å)[24] and a CH−O hydrogen bond (2.354 Å) exist on the A and B rings of **1**·H in addition to the main NH−O hydrogen bonds (shown in red, Figure 4a). The introduction of electron-withdrawing F atom on the Ph group of **1** increases the acidity of the CH group to strengthen the CH−O hydrogen bonds and further stabilize **TS3rs**. This is consistent with the experimentally observed substituent effects of **1**.[9] These rational hydrogen bonding networks and the additional attractive dispersion interaction result in the stability of **TS3rs** being higher than those of the other diastereomeric TSs. In contrast, unfavorable steric interactions of the 2,6-$(MeO)_2C_6H_3$ group of **2** and the pyrrole ring of **3** with the B rings of **1**·H weaken the main NH−O hydrogen bonds (1.872 and 1.776 Å), thereby destabilizing **TS3sr** (shown by curved purple line, Figure 4b). The significant steric repulsion between the B ring and the *i*-Bu group of **1**·H and the Bn and 2,6-$(MeO)_2C_6H_3$ groups of **2** reduces the main NH−O hydrogen bonding interactions

DOI: 10.1021/acs.joc.6b02572
J. Org. Chem. 2017, 82, 541−548

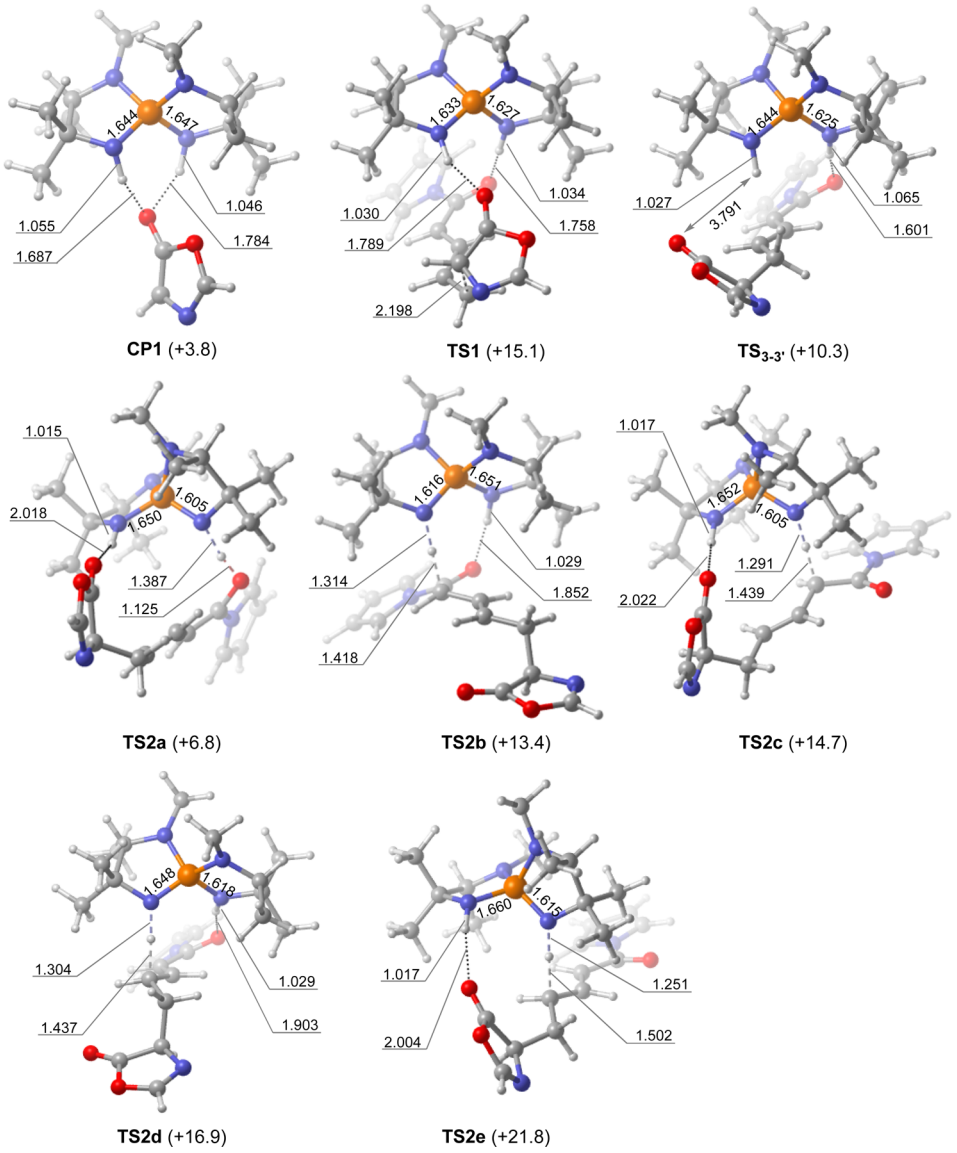

Figure 2. 3D structures of the ion-pair complex (**CP1**), the C−C bond formation (**TS1**), the C^{γ}-C^{δ} bond rotation ($TS_{3-3'}$), and the *O*-/*C*-protonation (**TS2a**, **TS2b**, **TS2c**, **TS2d**, and **TS2e**). Relative Gibbs free energies are shown in parentheses (kcal/mol). Bond lengths are shown in Å.

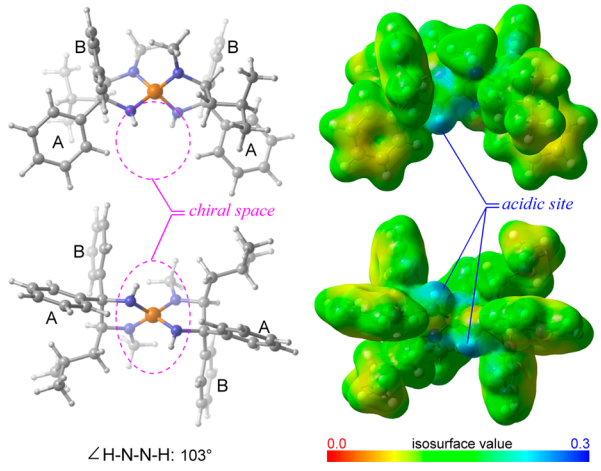

Figure 3. Front and bottom views of 3D structure and electrostatic potentials of protonated *P*-spiro phosphorene **1**·H.

(1.852 and 1.745 Å) and thus destabilizes **TS3rr** (shown by curved purple line, Figure 4d). Computational results suggest that **TS3sr** and **TS3rr** become more destabilized with increasing bulkiness of the alkyl substituent (R) in **1** and the aryl substituent (Ar^1) in **2**. This is qualitatively consistent with the experimentally observed tendency of the substituent effects of **1** and **2**.[9] In a manner similar to that of **TS3rs**, both **2** and **3** are well-oriented in the chiral space in **TS3ss** without any significant unfavorable steric interactions (Figure 4c). Although the main NH−O hydrogen bonds efficiently form, there are no additional and notable CH−π and CH−O interactions in **TS3ss**.[25] These computational results indicate that the attractive interactions between **1**·H and **2** and **3** are the fundamental factors that determine the stability of the diastereomeric TSs

To elucidate the origin of the high 1,6-selectivity, diastereomeric TSs in the 1,4-addition of **2**·H to **3** (**TS4**) were explored and compared with those of **TS3**. Four diastereomeric TSs in the 1,4-addition (**TS4rs**, **TS4sr**, **TS4rr**, and **TS4ss**)[26] are located at energy levels higher than that of

DOI: 10.1021/acs.joc.6b02572
J. Org. Chem. 2017, 82, 541−548

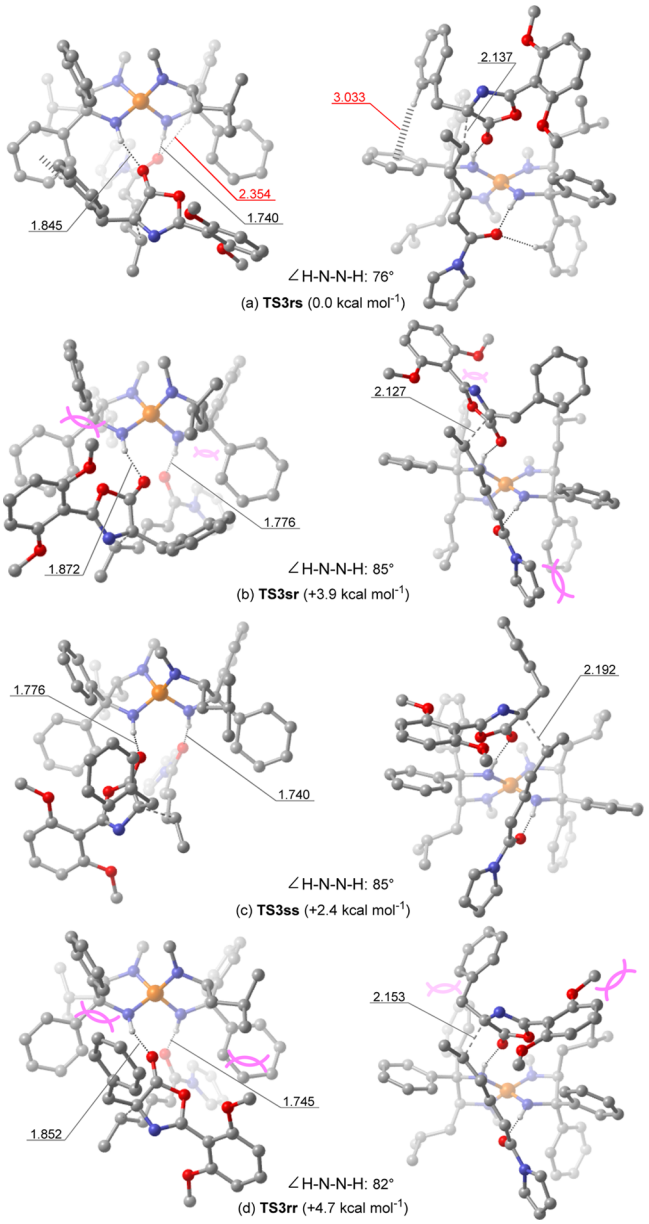

Figure 4. Front and bottom views of 3D structures and the relative Gibbs free energies of (a) **TS3rs**, (b) **TS3sr**, (c) **TS3ss**, and (d) **TS3rr**.

TS3 in agreement with the experimentally observed high 1,6-selectivity. In contrast to **TS3**, the most stable TS among the four diastereomeric TSs is **TS4ss**, in which the facial selectivity of **2** is reversed relative to that of the most stable **TS3rs** (Figure 5). The difference in the electrophilic carbon center of **3** (e.g., C^{β}) induces significant structural changes, in particular, the relative orientation of **3**, in the diastereomeric TSs albeit retaining the strong main NH−O hydrogen bonds whose lengths range from ca. 1.7−1.9 Å (Figure S4 in the Supporting Information). No steric repulsion is noted between **1**·H and **2** and **3** in **TS4ss**. In comparison with **TS3ss**, the *N*-acyl group is close to the phosphonium center of **1**·H to form the CH−O hydrogen bond (2.171 Å), thereby stabilizing **TS4ss**. The two NH residues of **1**·H forming the NH−O hydrogen bonds are considerably distorted in **TS4ss** (H−N−N−H dihedral angle: 55°) relative to the optimized **1**·H structure (H−N−N−H dihedral angle: 103°).

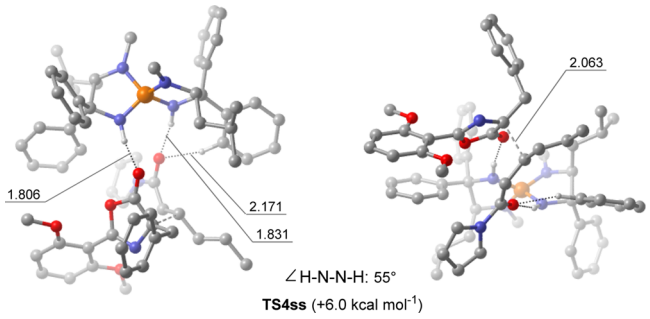

Figure 5. Front and bottom views of 3D structure of **TS4ss**. The relative Gibbs free energy of **TS4ss** to **TS3rs** is shown in parentheses.

To identify the main factor in controlling regio- and stereoselectivities, the distortion/interaction analysis[27] of diastereomeric TSs was carried out (Table 1). The high

Table 1. Distortion/Interaction Analysis of TS3rs, TS3sr, TS3ss, TS3rr, and TS4ss

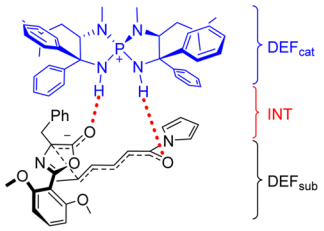

TS	ΔDEF_{cat}	ΔDEF_{sub}	ΔINT
$TS3_{rs}$	0.0	0.0	0.0
$TS3_{sr}$	0.1	0.1	3.9
$TS3_{ss}$	0.5	0.1	3.5
$TS3_{rr}$	0.0	0.0	3.8
$TS4_{ss}$	2.2	4.2	1.1

$\Delta DEF = DEF(TS) - DEF(TS3_{rs})$ /kcal mol^{-1}
$\Delta INT = INT(TS) - INT(TS3_{rs})$ /kcal mol^{-1}

stereoselectivity (**TS3rs** vs **TS3sr**, **TS3ss**, and **TS3rr**) is mainly due to the interaction energy difference between **1**·H and **2** and **3** (ΔINT). Whereas ΔINT has a large impact on the relative stability of diastereomeric **TS3** structures, the distortion energy difference (ΔDEF_{cat} and ΔDEF_{sub}) exerts little influence. This is attributed to the notable structural features that **1**·H has the rigid chiral space (Figure 3) and **2** and **3** have highly conjugated structures. In contrast to stereoselectivity control, ΔDEF_{sub} preferentially contributes to the high 1,6-selectivity (**TS3rs** vs **TS4ss**). The 1,4-addition disrupts the π-conjugated system between C═C and C═O bonds in **3**, inducing significantly large ΔDEF_{sub} in **TS4ss**.

We further addressed the high regioselectivity in the 1,8-addition of **2**·H to **4** catalyzed by **1**. Diastereomeric TS structures related to the 1,8- (**TS5**), 1,6- (**TS6**), and 1,4-addition (**TS7**) were explored based on the realistic model study of the 1,6-addition system (Figure 6). As a preliminary study, the diastereomeric TSs, including all s-*trans*, s-*trans*/s-*cis*, and all s-*cis* conformers of **4**, were explored using the simplified chemical model (Figure S5 in the Supporting Information). On the basis of the most stable TS, including all s-*trans* conformer of **4**, the relative energies of the most stable diastereomeric TSs for 1,8- (**TS5rs**), 1,6- (**TS6rs**), and 1,4-addition (**TS7ss**) were compared. **TS5rs** is the most stable TS, in good agreement with the preference for the 1,8-addition observed in the experimental results. As expected from the experimental results leading to the same absolute structure of the major enantiomer in both 1,8- and 1,6-addition systems, a similar structural tendency is found in both **TS5** and **TS6**. Both **2** and **4** fit the chiral space well with additional CH−π and CH−O interactions in **TS5rs** and **TS6rs**, respectively (Figures 6a and b). Diastereomeric **TS7** structures have structural properties similar to that of **TS4**, and **TS7ss** is the most stable (Figure 6c). The distortion/interaction analysis

DOI: 10.1021/acs.joc.6b02572
J. Org. Chem. 2017, 82, 541−548

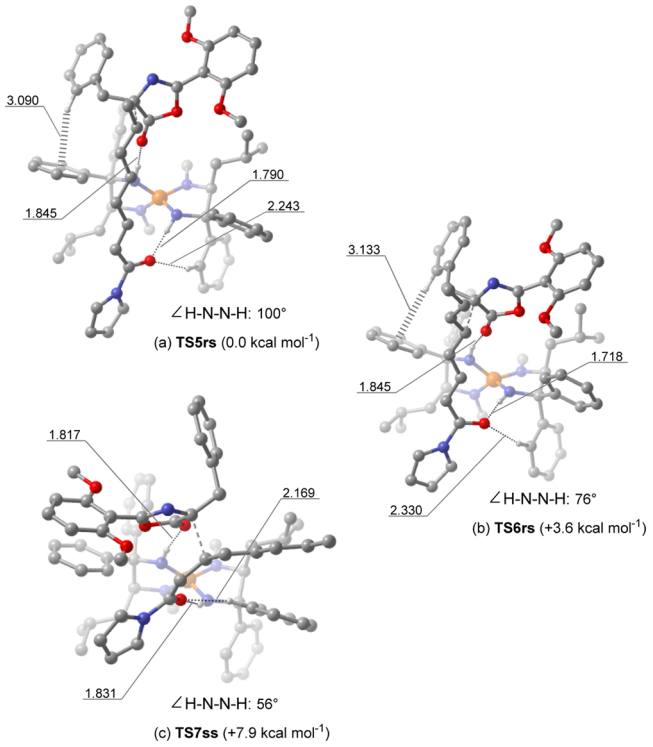

Figure 6. Front views of 3D structures and the relative Gibbs free energies of (a) **TS5rs**, (b) **TS6rs**, and (c) **TS7ss**.

indicates that distortion energy differences (ΔDEF_{cat}, ΔDEF_{sub}) significantly contribute to the relative stability of the diastereomeric TSs (Figure 7). The large ΔDEF_{sub} of **TS6rs** and **TS7ss** in particular are attributed to distortion destabilization through the disruption of the π-conjugated system between C═C and C═O bonds. On the other hand, ΔDEF_{cat} of **TS6rs** and **TS7ss** makes a non-negligible contribution to the relative stability of the diastereomeric TSs. The two NH residues of **1**·H forming the NH−O hydrogen bonds are considerably distorted from the optimized **1**·H structure (H−N−N−H dihedral angle: 103°) in the order of **TS7ss** (56°) > **TS6rs** (76°) > **TS5rs** (100°). The dihedral angle between the two NH residues depends on the distance between the two oxygen atoms of **2** and **4**. In **TS5rs**, the relative orientation of **2** and **4** is suitable for the optimized location of the two NH residues of **1**·H.

CONCLUSION

DFT calculations of the asymmetric 1,6- and 1,8-additions of **2**·H to **3** and **4** catalyzed by **1** were carried out to elucidate the whole reaction mechanism as well as the origin of the high regio- and stereocontrolling ability of **1**. The rate- and stereodetermining C−C bond formation (**TS1**) proceeds through the formation of phosphonium-enolate ion-pair complexes (**CP1**, and **CP2**). The C^{α}-protonation of the resulting enolate anion (**TS2b** and **TS2c**) is energetically favored over the C^{γ}-protonation (**TS2d** and **TS2e**) involving a high energy barrier and the reversible *O*-protonation (**TS2a**). The C^{α}-protonated product is eventually obtained along with the regeneration of **1**. The high regio- and enantioselectivities in the 1,6-addition system are attributed to the notable steric and electronic features of **1**·H and **3**. The hydrogen bonds (NH−O and CH−O) and the attractive CH−π interaction between **1**·H and **2** and **3** play a crucial role in achieving high stereocontrol. There exist rational catalyst−substrate interaction networks with no unfavorable steric interactions in **TS3rs**, leading to the major enantiomer. Steric repulsion together with the narrow and rigid chiral space constructed by the four Ph groups of **1**·H decreases the NH−O hydrogen-bonding interaction and destabilizes other diastereomeric TSs, leading to the minor enantiomer and diastereomer. On the other hand, the distortion energy difference of **3** mainly contributes to the high regiocontrol. The large distortion of **3** in **TS4ss** (1,4-addition) originates in the disruption of the π-conjugated system. In a manner similar to that of the 1,6-addition system, the catalyst-substrate interaction networks are a fundamental factor in controlling stereoselectivity in the 1,8-addition system. The high 1,8-selectivity is achieved by the destabilization of **TS6rs** (1,6-addition) and **TS7ss** (1,4-addition), consisting of the structurally and electronically distorted **1**·H and **4**, respectively. These computational results provide deep insight into the high regio- and stereocontrolling ability of the precisely designed **1**.

EXPERIMENTAL SECTION

General Information. All physical data regarding to the following reactions (preparation of iminophosphorane **1a** and 1,6-adduct **5a**) were collected by the same instruments as in our previous paper.[9]

Procedure for Preparation of Iminophosphorane 1a (−1∼ >99% ee). An appropriate ratio mixture of chiral tetraaminophosphonium chlorides (*P*,*S*)-**1a**·HCl and (*M*,*R*)-**1a**·HCl was placed into a sample tube, and the mixture was dissolved into methanol. The methanolic solution was passed through a column of ion-exchange resin (Amberlyst A-26 OH form) to afford a solution of iminophosphorane **1a** (−1∼ >99% ee). The resulting solution was concentrated by rotary evaporation, and residual solid was washed with

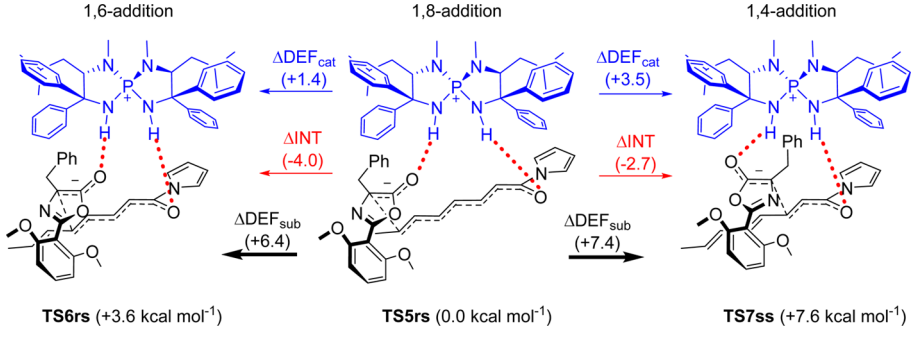

Figure 7. Distortion/interaction analysis of **TS5rs**, **TS6rs**, and **TS7ss**.

DOI: 10.1021/acs.joc.6b02572
J. Org. Chem. 2017, 82, 541−548

deionized water on a funnel. The solid thus obtained was dried under reduced pressure to afford the iminophosphorane **1a** as a white solid. Enantiomeric excess of iminophosphorane **1a** was checked as follows. A mixture of iminophosphorane **1a** (−1∼ >99% ee) and chiral phosphoric acid (*R*)-**CPA** was dissolved into $CDCl_3$. Enantiomeric excess of **1a** was determined by the integration ratio of diastereomeric phosphonium salts in ^{31}P NMR (see the Supporting Information).

Experimental Procedure for Investigating Correlation between the Enantiomeric Excess of Catalyst 1a and that of the 1,6-Adduct 5a. Azlactone **2a**·H (25.13 mg, 0.10 mmol) and dienylacylpyrrole **3a** (17.73 mg, 0.11 mmol) was dissolved into toluene (1.0 mL) under Ar atmosphere. Chiral iminophosphorane **1a** (3.40 mg, 5.0 μmol) was added portionwise at 0 °C, and the resulting reaction mixture was stirred for 3 h. The reaction was quenched by the addition of a solution of trifluoroacetic acid in toluene (0.5 M, 50.0 μL), and all volatiles were removed under reduced pressure to give a crude residue. The diastereomeric ratio of **5a** was determined by ^1H NMR analysis (400 MHz). Subsequent purification by column chromatography on silica gel (H/EA = 1/1 as eluent) gave the adducts in >99% yield as a mixture of isomers. The enantiomeric excess of 1,6-adduct **5a** was determined by HPLC analysis (see the Supporting Information).

■ ASSOCIATED CONTENT

Supporting Information

The Supporting Information is available free of charge on the ACS Publications website at DOI: 10.1021/acs.joc.6b02572.

Experimental and computational details, including Cartesian coordinates and absolute energies for stationary points (PDF)

■ AUTHOR INFORMATION

Corresponding Author

*E-mail: myamanak@rikkyo.ac.jp.

ORCID

Masahiro Yamanaka: 0000-0001-7978-620X

Ken Sakata: 0000-0002-6920-0735

Notes

The authors declare no competing financial interest.

■ ACKNOWLEDGMENTS

This work was supported by a Grant-in-Aid for Scientific Research on Innovative Areas "Advanced Molecular Transformations by Organocatalysts" from MEXT, Scientific Research (C) from JSPS, and MEXT-Supported Program for the Strategic Research Foundation at Private Universities. K.Y. acknowledges a Grant-in-Aid for JSPS Fellows.

■ REFERENCES

(1) (a) Leonard, J.; Díez-Barra, E.; Merino, S. *Eur. J. Org. Chem.* **1998**, *10*, 2051. (b) Chen, F.; Gong, P.; Gao, Y.; Zhang, H.; Zhou, A. *Mini-Rev. Org. Chem.* **2013**, *10*, 207. (c) Heravi, M. M.; Hajiabbasi, P.; Hamidi, H. *Curr. Org. Chem.* **2014**, *18*, 489. (d) Byrd, K. M. *Beilstein J. Org. Chem.* **2015**, *11*, 530.

(2) For recent, excellent reviews on asymmetric 1,6-addition reactions, see: (a) Csákÿ, A. G.; de la Herrán, G.; Murcia, M. C. *Chem. Soc. Rev.* **2010**, *39*, 4080. (b) Biju, A. T. *ChemCatChem* **2011**, *3*, 1847. (c) Silva, E. M. P.; Silva, A. M. S. *Synthesis* **2012**, *44*, 3109. (d) Lear, M. J.; Hayashi, Y. *ChemCatChem* **2013**, *5*, 3499.

(3) Fuson, R. C. *Chem. Rev.* **1935**, *16*, 1.

(4) For recent, selected examples of asymmetric 1,4-additions to electron-deficient dienes, see: (a) Agostinho, M.; Kobayashi, S. *J. Am. Chem. Soc.* **2008**, *130*, 2430. (b) Trost, B. M.; Hitce, J. *J. Am. Chem. Soc.* **2009**, *131*, 4572. (c) Shepherd, N. E.; Tanabe, H.; Xu, Y.; Matsunaga, S.; Shibasaki, M. *J. Am. Chem. Soc.* **2010**, *132*, 3666. (d) Huang, H.; Jin, Z.; Zhu, K.; Liang, X.; Ye, J. *Angew. Chem., Int. Ed.* **2011**, *50*, 3232. (e) Gremaud, L.; Alexakis, A. *Angew. Chem., Int. Ed.* **2012**, *51*, 794. (f) Hayashi, Y.; Okamura, D.; Umemiya, S.; Uchimaru, T. *ChemCatChem* **2012**, *4*, 959.

(5) For selected examples of chiral transition-metal complex-catalyzed enantioselective 1,6-additions of carbanionic nucleophiles to α,β,γ,δ-unsaturated systems, see: (a) Hayashi, T.; Yamamoto, S.; Tokunaga, N. *Angew. Chem., Int. Ed.* **2005**, *44*, 4224. (b) Nishimura, T.; Yasuhara, Y.; Hayashi, T. *Angew. Chem., Int. Ed.* **2006**, *45*, 5164. (c) Hénon, H.; Mauduit, M.; Alexakis, A. *Angew. Chem., Int. Ed.* **2008**, *47*, 9122. (d) den Hartog, T.; Huang, Y.; Fañanás-Mastral, M.; Meuwese, A.; Rudolph, A.; Pérez, M.; Minnaard, A. J.; Feringa, B. L. *ACS Catal.* **2015**, *5*, 560 and references cited therein..

(6) For examples of organocatalytic asymmetric 1,6-additions, see: (a) Bernardi, L.; López-Cantarero, J.; Niess, B.; Jørgensen, K. A. *J. Am. Chem. Soc.* **2007**, *129*, 5772. (b) Wei, Y.; Liu, Z.; Wu, X.; Fei, J.; Gu, X.; Yuan, X.; Ye, J. *Chem. - Eur. J.* **2015**, *21*, 18921. (c) Gu, X.; Guo, T.; Dai, Y.; Franchino, A.; Fei, J.; Zou, C.; Dixon, D. J.; Ye, J. *Angew. Chem., Int. Ed.* **2015**, *54*, 10249. (d) Zhao, K.; Zhi, Y.; Wang, A.; Enders, D. *ACS Catal.* **2016**, *6*, 657 and references cited therein..

(7) (a) Lee, K.-s.; Hoveyda, A. H. *J. Am. Chem. Soc.* **2010**, *132*, 2898. (b) Tian, X.; Liu, Y.; Melchiorre, P. *Angew. Chem., Int. Ed.* **2012**, *51*, 6439. (c) Akagawa, K.; Nishi, N.; Sen, J.; Kudo, K. *Org. Biomol. Chem.* **2014**, *12*, 3581. (d) Kowalczyk, R.; Boratyński, P. J.; Wierzba, A. J.; Bąkowicz, J. *RSC Adv.* **2015**, *5*, 66681. (e) Dou, Q.-Y.; Tu, Y.-Q.; Zhang, Y.; Tian, J.-M.; Zhang, F.-M.; Wang, S.-H. *Adv. Synth. Catal.* **2016**, *358*, 874.

(8) (a) Sun, H.-W.; Liao, Y.-H.; Wu, Z.-J.; Wang, H.-Y.; Zhang, X.-M.; Yuan, W.-C. *Tetrahedron* **2011**, *67*, 3991. (b) Murphy, J. J.; Quintard, A.; McArdle, P.; Alexakis, A.; Stephens, J. C. *Angew. Chem., Int. Ed.* **2011**, *50*, 5095.

(9) Uraguchi, D.; Yoshioka, K.; Ueki, Y.; Ooi, T. *J. Am. Chem. Soc.* **2012**, *134*, 19370.

(10) For examples of nonstereoselective 1,8-addition reactions, see: (a) Barbot, F.; Kadib-Elban, A.; Miginiac, P. *J. Organomet. Chem.* **1988**, *345*, 239. (b) Koop, U.; Handke, G.; Krause, N. *Liebigs Ann.* **1996**, *1996*, 1487. (c) Brocchini, S. J.; Lawton, R. G. *Tetrahedron Lett.* **1997**, *38*, 6319.

(11) Triaminoiminophosphoranes are known as a P1-phosphazenes, which were developed by Schwesinger, see: (a) Schwesinger, R.; Schlemper, H. *Angew. Chem., Int. Ed. Engl.* **1987**, *26*, 1167. For a review, see: (b) Ishikawa, T. *Superbases for Organic Synthesis: Guanidines, Amidines, Phosphazenes and Related Organocatalysts*; John Wiley & Sons: West Sussex, U.K., 2009.

(12) For a review on organic base catalysis, see: Palomo, C.; Oiarbide, M.; López, R. *Chem. Soc. Rev.* **2009**, *38*, 632.

(13) For reviews on phosphonium salt catalysis, see: (a) Werner, T. *Adv. Synth. Catal.* **2009**, *351*, 1469. (b) Enders, D.; Nguyen, T. V. *Org. Biomol. Chem.* **2012**, *10*, 5327.

(14) (a) Uraguchi, D.; Ooi, T. *Yuki Gosei Kagaku Kyokaishi* **2010**, *68*, 1185. (b) Uraguchi, D.; Ueki, Y.; Ooi, T. *Chem. Sci.* **2012**, *3*, 842. (c) Corbett, M. T.; Uraguchi, D.; Ooi, T.; Johnson, J. S. *Angew. Chem., Int. Ed.* **2012**, *51*, 4685. (d) Uraguchi, D.; Tsutsumi, R.; Ooi, T. *J. Am. Chem. Soc.* **2013**, *135*, 8161. (e) Uraguchi, D.; Yamada, K.; Ooi, T. *Angew. Chem., Int. Ed.* **2015**, *54*, 9954. (f) Horwitz, M. A.; Tanaka, N.; Yokosaka, T.; Uraguchi, D.; Johnson, J. S.; Ooi, T. *Chem. Sci.* **2015**, *6*, 6086.

(15) For reviews of azlactones in organic syntheses, see: (a) Fisk, J. S.; Mosey, R. A.; Tepe, J. J. *Chem. Soc. Rev.* **2007**, *36*, 1432. (b) Mosey, R. A.; Fisk, J. S.; Tepe, J. J. *Tetrahedron: Asymmetry* **2008**, *19*, 2755. (c) Alba, A.-N. R.; Rios, R. *Chem. - Asian J.* **2011**, *6*, 720.

(16) Frisch, M. J.; et al.. *Gaussian 09*, revision D.01; Gaussian, Inc.: Wallingford, CT, 2013.

(17) (a) Becke, A. D. *J. Chem. Phys.* **1993**, *98*, 5648. (b) Lee, C.; Yang, W.; Parr, R. G. *Phys. Rev. B: Condens. Matter Mater. Phys.* **1988**, *37*, 785.

(18) The energy profile in solution using polarizable continuum model (PCM) is shown in the Supporting Information.

DOI: 10.1021/acs.joc.6b02572
J. Org. Chem. 2017, 82, 541−548

(19) (a) Grimme, S. *J. Comput. Chem.* **2006**, *27*, 1787. (b) Ehrlich, S.; Moellmann, J.; Grimme, S. *Acc. Chem. Res.* **2013**, *46*, 916.
(20) Legault, C. Y. *CYLview*, 1.0b; Université de Sherbrooke: Canada, 2009.
(21) Simón, L.; Paton, R. S. *J. Org. Chem.* **2015**, *80*, 2756.
(22) For C^{α}- and C^{γ}-protonation in **TS2b** and **TS2d** to occur, the hydrogen bond between the positively charged NH residue of **Cat**·H and **AZ** needs to dissociate. Therefore, C^{α}- and C^{γ}-protonation in **TS2b** and **TS2d** proceeds after breaking the hydrogen bond through the C^{γ}-C^{δ} bond rotation (**TS$_{3-3'}$**) followed by generating **CP3′** as the directly connected complex to **TS2b** and **TS2d**.
(23) Diasteromers of product should be stereoselectively obtained; however, it was not supplied with sufficient quantities for determining the enantiomeric excess.
(24) The attractive CH−π interaction contributes to increase the catalyst−substrate interaction energy. The detailed computational analysis is shown in the Supporting Information.
(25) Whereas the CH−O hydrogen bonds on the A and B rings are in the range of ca. 2.5−2.8 Å, there is geometrically no possibility of the CH−π and π−π interactions in **TS2ss**.
(26) The details are shown in the Supporting Information.
(27) The energies of **TS-S** and **TS-R** were dissected into the distortion (DEF) and interaction energies (INT) for the two distorted fragments (catalyst and substrates) constructing TS. The differences for each energy (ΔDEF and ΔINT) between diastereomeric TSs were calculated by the counterpoise method at the B3LYP-D3/6-31+G** level. For the original distortion/interaction analysis, see: (a) Morokuma, K.; Kitaura, K. *Chemical Applications of Atomic and Molecular Electrostatic Potentials*; Politzer, P., Truhlar, D. G., Eds.; Plenum: New York, 1981. (b) Ess, D. N.; Houk, K. N. *J. Am. Chem. Soc.* **2007**, *129*, 10646. (c) Ess, D. H.; Houk, K. N. *J. Am. Chem. Soc.* **2008**, *130*, 10187. (d) Lam, Y.-H.; Cheong, P. H.-Y.; Blasco Mata, J. M.; Stanway, S. J.; Gouverneur, V. R.; Houk, K. N. *J. Am. Chem. Soc.* **2009**, *131*, 1947. (e) Paton, R. S.; Kim, S.; Ross, A. G.; Danishefsky, S. J.; Houk, K. N. *Angew. Chem., Int. Ed.* **2011**, *50*, 10366. (f) Green, A. G.; Liu, P.; Merlic, C. A.; Houk, K. N. *J. Am. Chem. Soc.* **2014**, *136*, 4575. (g) Yang, Y.-F.; Liang, Y.; Liu, F.; Houk, K. N. *J. Am. Chem. Soc.* **2016**, *138*, 1660.

DOI: 10.1021/acs.joc.6b02572
J. Org. Chem. 2017, 82, 541−548